Rapid Communications

Multiple shock reverberation compression of dense Ne up to the warm dense regime: Evaluating the theoretical models

J. Tang, Y. J. Gu,* Q. F. Chen,† Z. G. Li, J. Zheng, C. J. Li, and J. T. Li
National Key Laboratory of Shock Wave and Detonation Physics, Institute of Fluid Physics, CAEP, Mianyang 621900, China

(Received 4 February 2018; published 6 April 2018)

Multiple shock reverberation compression experiments are designed and performed to determine the equation of state of neon ranging from the initial dense gas up to the warm dense regime where the pressure is from about 40 MPa to 120 GPa and the temperature is from about 297 K up to above 20 000 K. The wide region experimental data are used to evaluate the available theoretical models. It is found that, for neon below 1.1 g/cm^3, within the framework of density functional theory molecular dynamics, a van der Waals correction is meaningful. Under high pressure and temperature, results from the self-consistent fluid variational theory model are sensitive to the potential parameter and could give successful predictions in the whole experimental regime if a set of proper parameters is employed. The new observations on neon under megabar (1 Mbar $= 10^{11}$ Pa) pressure and eV temperature (1 eV $\approx 10^4$ K) enrich the understanding on properties of warm dense matter and have potential applications in revealing the formation and evolution of gaseous giants or mega-Earths.

DOI: 10.1103/PhysRevB.97.140101

Knowledge of thermodynamic properties of materials in a warm dense region is especially important for us to understand many high-energy density physics processes and phenomena, such as the interior structure of the earth [1,2], inertial confinement fusion [3], and the formation and evolution of supernovas [4] and gaseous giants [5–7]. Because of the simple filled-shell electronic configuration, neon (Ne) and other rare gases can be well used as standard test cases for the thermodynamic properties studies, including the equation of state (EOS), metallic transition, and so on, in a warm dense region. Particularly, of all the rare gases, Ne is the second element, and it can act as an important bridge from the simplest helium (He) to complex argon (Ar), krypton (Kr), and xenon (Xe) for developing warm dense matter (WDM) theory models. Moreover, Ne is the primary constituent of planetary and stellar atmospheres. Its thermodynamic properties in the WDM region are also vital to construct the inner structure of these astrophysics objects and understand their formation and evolution, which have attracted increasing interest in astrophysics studies [8,9]. Various theoretical models, including self-consistent fluid variational theory (SFVT) [10], density functional theory molecular dynamics (DFT-MD) [8,11], and path-integral Monte Carlo [11], have been developed to predict the thermophysical properties of Ne under warm dense conditions. In Ne, some unexpected unnatural properties, including the widest energy gap, the highest metallization pressure, and an opposite density dependency of a band gap under compression [12–15], were observed. These anomalous behaviors were deemed to probably relate to the unique and strong bounded two shells of the electronic orbit of Ne [16]. Such a unique electronic shell structure may lead to different shock compression responses of Ne compared with other rare gases especially in the WDM region. It prompts the need for an improved understanding of Ne's behavior at this extreme condition. The shock compression response of other rare gases He, Ar, Kr, and Xe had been extensively studied by experiments [17–29] while neon had received less attention. So, in this Rapid Communication, we designed and performed a series of shock experiments on neon by a shock reverberation technique, and presented the novel experimental EOSs of dynamically compressed dense gaseous Ne into the WDM regime (beyond 100 GPa) for evaluating the existing theoretical models and verifying the anomalous behavior prediction by these theoretical models. The obtained wide-range EOS results, including principal- and off-Hugoniot states in the 10–20-GPa regime, provide a useful evaluation for current fundamental theoretical methods and models in the WDM region. The achieved ~120-GPa pressure is also directly relevant to the interiors of gas giant planets and is helpful for revealing the formation and evolution of these giant planets.

A series of shock reverberation experiments on Ne was conducted using a two-stage light gas gun with a bore diameter of 30 mm, which produces much longer time scales (microseconds) and much larger sizes (grams or cm^3 volumes) of WDM with uniform constant density, pressure, and temperature that can be achieved and sustained, and allows a better diagnosis of WDM with these temporal and spatial scales [30]. The gaseous Ne was precompressed up to ~40 MPa at room temperature for obtaining a high initial density gaseous sample, which allows high pressure to be achieved. The process of shock reverberation compression is implemented by the confinement of Ne between two high shock impedance materials including a 304 steel base plate (S304) and a composite window consisting of an ~0.1-mm aluminum (Al) foil, an ~4-mm-thick lithium fluoride (LiF) anvil, and an ~2-mm-thick sapphire (Al_2O_3) sheet. The experimental configuration is analogous to the one used in our previous work on He [17]. Using the two-stage light gas gun, an ~3.2-mm-thick tantalum (Ta) flyer was accelerated

*guyunjun01@163.com
†chenqf01@gmail.com

up to 4.5 ∼ 6.1 km/s. The flyer velocity was measured by a magnetoflyer velocity system with an accuracy of about 1%. A planar strong shock wave was produced when the Ta flyer impacted on the front surface of the S304 baseplate. The shock wave will transmit into Ne across the S304 and then propagate and reverberate repeatedly between the S304 and the composite window due to its higher shock impedance than that of Ne. Increasing pressures, densities, and temperatures in Ne were created during shock reverberation compression. By the multiple shock reverberations, the dense gaseous Ne was compressed and entered into the warm dense regime.

A multichannel optical pyrometer (MCOP) was used to record the spectral radiance history of the shocked Ne within a wavelength ranging from 405 to 732 nm and two sets of Doppler pin systems (DPS-I and DPS-II) with an operating wavelength of 1550 nm were used to measure the velocity profiles of the shock front and the sample/composite window interface. Typical experimental records obtained from shot No. GNe15925 are shown in Fig. 1. The experimental records by the MCOP and DPS-I provide a clear indication of shock arrival at the S304/Ne interface (at time t_0) and the Ne/LiF interface (at time t_1). The flat region of the MCOP signals between times t_0 and t_1 implies that the shock wave transmits across Ne with a steady state, which corresponds to the first shock process of Ne. The apparent shock velocity v_a of the first shocked Ne can be directly read from DPS-I. The v_a-combined refractive index n_0 of the unshocked Ne at the 1550-nm wavelength was used to deduce the true shock velocity [31] $U_{s,1} = v_a/n_0$. n_0 was measured with the aid of an optical-fiber frequency domain interferometer device [32] before experiments, which is described in the Supplemental Material (SM) [33]. $U_{s,1}$ can also be acquired by the shock transit time (t_1-t_0) recorded by the MCOP and DPS-I along with the initial sample thickness, which can provide a cross-check in our experiments. The DPS-II records provide the shock breakout time (t_1 and t_2) and the step-rise particle velocities ($U_{p,2}$ and $U_{p,4}$) when the shock wave is reflected at the Ne/LiF interface [see Fig. 1(b)]. After obtaining the values of $U_{s,1}$, $U_{p,2}$, $U_{p,4}$, t_0, t_1, and t_2, we can deduce the shock states of Ne from the first to the fourth shock compression using a Monte Carlo impedance matching method [28,29,34–36] together with the known Hugoniots of Ta, S304, and LiF [37,38]. Furthermore, according to the values of h_i recorded by the MCOP at eight wavelengths combing with their calibrating data, the first shock temperatures can be extracted to be about 1.9 ∼ 2.4 × 10^4 K with a 1σ uncertainty of ∼6.8% by fitting the eight-channel data to the Planck gray body radiation spectrum [39]. The detailed data analyzing and processing are referred to in our provided SM [33].

A total of four experimental shots on Ne were performed, covering wide pressure and density ranges of 40 MPa–120 GPa and 0.269–3.4 g/cm^3. The obtained experimental EOSs for the four shots are listed in Table IV of the SM [33]. By using shock reverberation technique, the gaseous Ne is successfully compressed into the megabar pressure region and the principal and off-Hugoniots are obtained in a single shot. An ∼12-fold high compression ratio (ρ/ρ_0) relative to the initial state is achieved. As mentioned in Ref. [40], compared with the traditional principal-Hugoniot experiment, the reshock measurements can remarkably magnify the differences in the observable quantities. So, the present multishock compression results are helpful for distinguishing the small differences in the EOS models, which can provide a useful evaluation for current theoretical models and methods. In order to evaluate the current available theoretical models, both the DFT-MD and the SFVT were used to simulate the multishock states of Ne corresponding with our experimental conditions in the shot of GNe15925. The EOS simulation results and the obtained experimental data were plotted in Fig. 2 as shock pressure versus compressed density for comparisons. Here, for clarity, only two shots of experimental data, corresponding to GNe15924 and GNe15925, are shown in Fig. 2. It is noted that the SFVT used here is a multicomponent chemical equilibrium model where the ionization of Ne is taken into account and the detailed description could see our previous work [10].

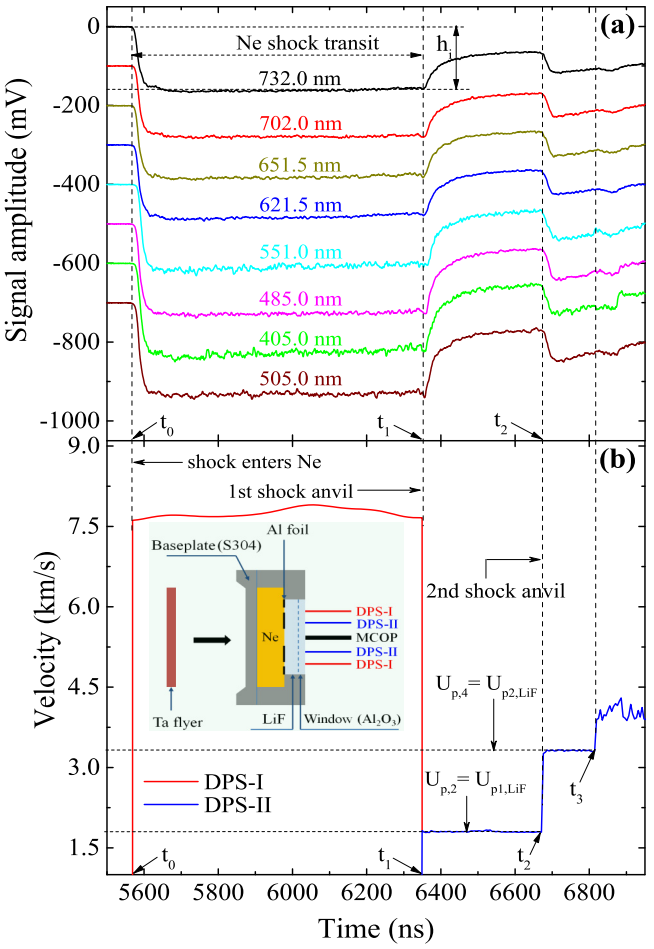

FIG. 1. Typical signals of the MCOP and the DPS for the shot of GNe15925: (a) The light radiation histories measured by the MCOP, and the intensity of light radiation represented by the voltage signal. The wavelengths are listed at 732.0 nm (0), 702.0 nm (−100), 651.5 nm (−200), 621.5 nm (−300), 551.0 nm (−400), 485.0 nm (−500), 405.0 nm (−600), and 505.0 nm (−700), the numbers in parentheses are the signal amplitude shifts, (b) the velocity recorded by the DPS, the red and blue curves are the shock velocity and the interface particle velocity history from DPS-I and DPS-II, respectively. The inset shows a schematic of the experimental configuration (dimensions are not to scale). The detailed description and the arrangement of the diagnostic probes could be seen in Sec. A in the Supplemental Material [33].

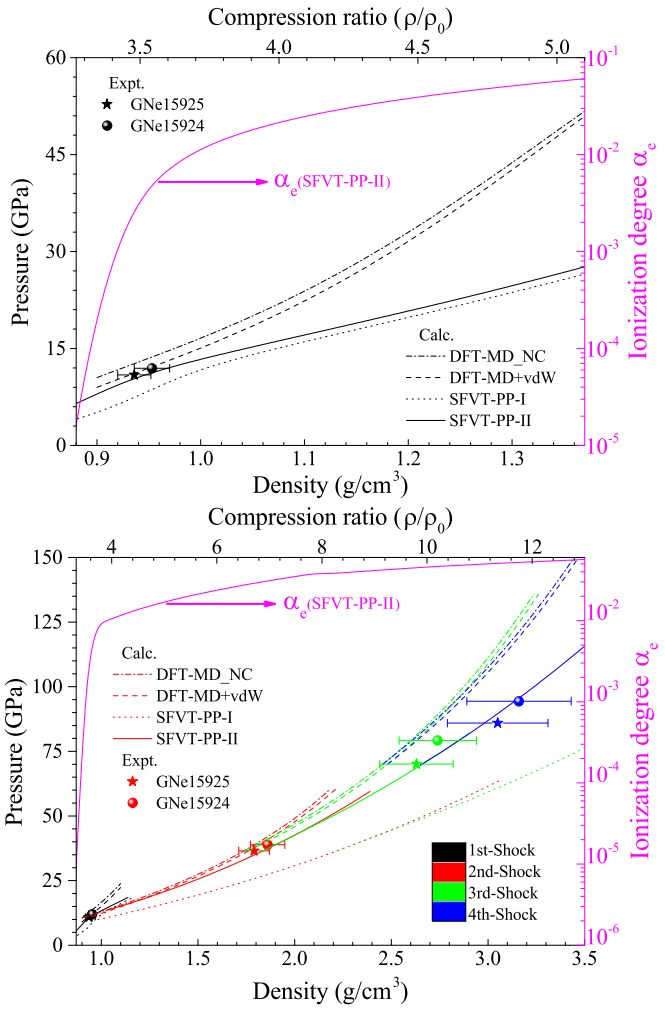

FIG. 2. Principle Hugoniot (up pattern) and multishock states (bottom pattern) of dense neon on the ρ-P plane.

The ionization degree (α_e) calculated by the SFVT is also shown in Fig. 2 as a function of density. In the DFT-MD, both the simulations with and without van der Waals (vdW) correction consideration were performed, which is labeled as DFT-MD + vdW and DFT-MD_NC, respectively. The vdW correction is based on a semiempirical force field method and is named DFT-D2 [41–43]. In the SFVT, two sets of different potential parameters, taken from Refs. [44,45], respectively, were used. The results were labeled as SFVT-PP-I and SFVT-PP-II, respectively. The DFT-MD simulations were performed with the VASP code [46–49] using the projector augmented-wave potential [50,51] and the Perdew-Burke-Ernzerhof exchange-correlation functional [52,53]. All computational details are given in the SM [33]. For the DFT-MD results, we can clearly see that the DFT-MD + vdW predicts a softer compression curve than that of the DFT-MD_NC especially for the first shock compression, and the differences between the two DFT-MD results get smaller with increasing density. For the SFVT results, we observe that they strongly rely on the potential parameters used. The results, SFVT-PP-I and SFVT-PP-II, show distinct deviations, and the deviations become larger and larger with increasing density. Comparing with the experiments, the SFVT-PP-II can well reproduce the experimental ρ-P data of Ne up to the fourth shock compression in the error bar range, whereas the SFVT-PP-I is found to greatly depart from the experiments. The possible reason as follows. The potential parameter I [44], not considering the thermal electronic excitation and ionization at high temperatures, was obtained by fitting the experimental solid neon isotherms at low temperatures (<300 K), which maybe is not applicable of characterizing behavior of the dynamically compressed Ne where a high shock temperature was contained. Both the DFT-MD + vdW and the DFT-MD_NC can give a satisfying prediction for the second shocked Ne, but, for the first shock compression, only the former shows good agreement with the experiments, which indicates the vdW correction plays an important role in Ne in the low-density region and has a weak effect under higher density. However, for the third and fourth shocks, both the two DFT-MD results obviously overestimate the pressure and deviate from the present experiments, whereas the SFVT-PP-II gives a softer result having better agreement with the experiments. The possible reasons are analyzed as below. The ionization degree calculated by the SFVT-PP-II becomes larger with increasing density. When the density is up to ~1.5 g/cm^3, the ionization degree achieves ~2% beyond which the two DFT-MD results begin to significantly depart from that of the SFVT calculation. The deviation becomes larger and larger with an increasing ionization degree. For the third and fourth shocks, the ionization degree is up to ~5%, and the deviation is up to about 10–20%. This indicates that considering ionization may be responsible for the fact that SFVT results are softer than those of thee DFT-MD. Thus, in order to improve the performance of the DFT-MD in the high-density region, the ionization may have to be considered. Similar conclusions were reported in Ref. [54] for He and were reported in Ref. [55] for Ar.

As mentioned in Ref. [56], temperature is an important constraint for EOS models. In our experiments, the shock temperatures along the principal Hugoniot of Ne in two shots of GNe15925 and GNe16527 were measured separately from shock pressure and density, which makes possible to further evaluate the applicability of the SFVT and the DFT-MD. Figure 3 shows the comparisons between the theoretical and the experimental results. It can be seen that the DFT-MD + vdW and the SFVT-PP-II results show reasonable agreements with the experiments, whereas those of the SFVT-PP-I depart significantly from the experiments, which are consistent with previous ρ-P comparisons. Unfortunately, in our experiments, shock temperature for above the first shock cannot be obtained because the LiF is ablated by shock-generated high temperatures at the Ne/LiF interface. Such high-temperature ablation greatly changes the optical transparency of the LiF and causes a decrease in the optical radiation intensity of shocked Ne under the second to fourth shock compressions relative to the first shock [see Fig. 1(a)]. So, we cannot obtain the shock temperatures corresponding to the last three compressions directly by the measured optical radiation signals or evaluate the validity of the EOS models under higher temperatures. It is well known that, in addition to the temperature and density, and other two dimensionless parameters, the coupling parameter $\Gamma = \frac{(Ze)^2}{k_B T}(\frac{4\pi}{3}n)^{1/3}$ and the degeneracy parameter $\Theta = \frac{2m_e k_B T}{\hbar}(3\pi^3 n_e)^{-2/3}$, are indispensable for characterizing

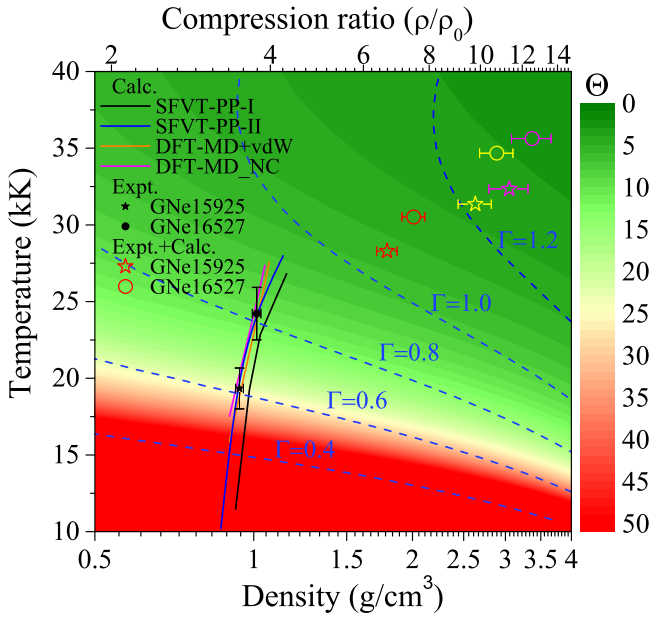

FIG. 3. The contours of degenerate (Θ) and coupling parameters (Γ) of dense neon on the ρ-P plane. The first shock temperatures determined by experiments (the black solid symbol) and theoretical models (the solid curves) are compared. The second to fourth shock temperatures are estimated with the SFVT-PP-II (the hollow symbol: the red, yellow, and magenta represent the second, third, and fourth shocks, respectively).

WDM's behavior. In order to judge whether or not the multishocked Ne in our experiments enters into the WDM regime, the shock temperatures for the second to fourth compressions Γ and Θ of Ne were estimated by the SFVT-PP-II, which were also plotted in Fig. 3. For the second to fourth compressions in our experiments, the coupling parameters are observed in the range of $\Gamma > 1$, and the Θ values are mostly around 1. This indicates that the present multishock compression states of Ne are mostly degenerate, strongly coupled, and nonideal. They have entered into the WDM regime, and these thermodynamic states are directly relevant to the interiors of gas giant planets. The obtained multishock experimental data on Ne are very useful not only for checking the thermodynamic models of WDM, but also for understanding material's responses to a wide range of physical environments.

In conclusion, we designed and performed a series of multiple shock reverberation compression experiments on Ne to probe its thermodynamic properties and to evaluate EOS models. This low-Z gas is successfully shocked from about 40 MPa up to megabar pressures in a single shot by a shock reverberation technique. The compression ratio of dense Ne is greatly enhanced with this technique. The designed comprehensive diagnostic system allows multiple objectives, including the shock velocity, particle velocity, and temperature to be measured and different experimental observables to be cross-checked in one shot. It provides an experimental paradigm which can increase output and decrease cost and allows for a more complete set of experimental observations. The obtained novel experimental EOSs provide an important benchmark for evaluating existing DFT-MD and SFVT in te WDM region, a means for evaluation of future theoretical developments, a new potential functional, a timely chance for further understanding on properties of warm dense matter, and for developing advanced interior, evolution, and dynamo models for solar and gaseous giants.

We thank our colleagues for the gas-gun operation, experimental diagnosis, and devices. We especially appreciate Prof. A. Xu and Dr. Y. H. Wang for helpful discussions. This Rapid Communication was supported by the National Natural Science Foundation of China (Grant No. 11674292), the Science Challenge Project (Grant No. TZ2016001), the Science and Technology Development Foundation of the China Academy of Engineering Physics (Grant No. 2015B0102001), the President Foundation of the China Academy of Engineering Physics (Grant No. 201501032), the Foundation of Laboratory of Shock Wave and Detonation Physics, CAEP (Grant No. 9140C670103150C67289), and the China Postdoctoral Science Foundation (Grant No. 2016M602928XB)

[1] K. P. Driver and B. Militzer, Phys. Rev. Lett. **108**, 115502 (2012).
[2] J. Dai, D. Kang, Z. Zhao, Y. Wu, and J. Yuan, Phys. Rev. Lett. **109**, 175701 (2012).
[3] S. X. Hu, L. A. Collins, T. R. Boehly, J. D. Kress, V. N. Goncharov, and S. Skupsky, Phys. Rev. E **89**, 043105 (2014).
[4] J. M. Lattimer, Annu. Rev. Nucl. Part. Sci. **31**, 337 (1981).
[5] M. D. Knudson, M. P. Desjarlais, A. Becker, R. W. Lemke, K. R. Cochrane, M. E. Savage, D. E. Bliss, T. R. Mattsson, and R. Redmer, Science **348**, 1455 (2015).
[6] B. Militzer and W. B. Hubbard, Astrophys. J. **774**, 148 (2013).
[7] W. J. Nellis, High Pressure Res. **37**, 119 (2017).
[8] H. F. Wilson and B. Militzer, Phys. Rev. Lett. **104**, 121101 (2010).
[9] J. Hughto, A. S. Schneider, C. J. Horowitz, and D. K. Berry, Phys. Rev. E **82**, 066401 (2010).
[10] Q. F. Chen, J. Zheng, Y. J. Gu, and Z. G. Li, Phys. Plasmas **22**, 122706 (2015).
[11] K. P. Driver and B. Militzer, Phys. Rev. B **91**, 045103 (2015).
[12] Y. G. He, X. Z. Tang, and Y. K. Pu, Physica B **405**, 4335 (2010).
[13] N. D. Drummond and R. J. Needs, Phys. Rev. B **73**, 024107 (2006).
[14] R. S. McWilliams, D. A. Dalton, Z. Konopkova, M. F. Mahmood, and A. F. Goncharov, Proc. Natl. Acad. Sci. USA **112**, 7925 (2015).
[15] J. C. Boettger, Phys. Rev. B **33**, 6788 (1986).
[16] J. Tang, Q. F. Chen, Z. J. Fu, Z. G. Li, W. L. Quan, Y. J. Gu, and J. Zheng, Phys. Plasmas **24**, 082709 (2017).
[17] J. Zheng, Q. F. Chen, Y. J. Gu, J. T. Li, Z. G. Li, C. J. Li, and Z. Y. Chen, Phys. Rev. B **95**, 224104 (2017).
[18] C. T. Seagle, W. D. Reinhart, A. J. Lopez, R. J. Hickman, and T. F. Thornhill, J. Appl. Phys. **120**, 125902 (2016).
[19] S. Brygoo, M. Millot, P. Loubeyre, A. E. Lazicki, S. Hamel, T. Qi, P. M. Celliers, F. Coppari, J. H. Eggert, D. E. Fratanduono, D. G. Hicks, J. R. Rygg, R. F. Smith, D. C. Swift, G. W. Collins, and R. Jeanloz, J. Appl. Phys. **118**, 195901 (2015).

[20] J. Eggert, S. Brygoo, P. Loubeyre, R. S. McWilliams, P. M. Celliers, D. G. Hicks, T. R. Boehly, R. Jeanloz, and G. W. Collins, Phys. Rev. Lett. **100**, 124503 (2008).
[21] J. Zheng, Q. Chen, Y. Gu, Z. Li, and Z. Shen, Sci. Rep. **5**, 16041 (2015).
[22] Q. F. Chen, J. Zheng, Y. J. Gu, Y. L. Chen, L. C. Cai, and Z. J. Shen, J. Chem. Phys. **140**, 074202 (2014).
[23] J. H. Carpenter, S. Root, K. R. Cochrane, D. G. Flicker, and T. R. Mattsson, Sandia Report No. SAND2012-7991, 2012 (unpublished), http://prod.sandia.gov/techlib/access-control.cgi/2012/127991.pdf.
[24] T. R. Mattsson, S. Root, A. E. Mattsson, L. Shulenburger, R. J. Magyar, and D. G. Flicker, Phys. Rev. B **90**, 184105 (2014).
[25] V. D. Glukhodedov, S. I. Kirshanov, T. S. Lebedeva, and M. A. Mochalov, J. Exp. Theor. Phys. **89**, 292 (1999).
[26] J. Zheng, Q. F. Chen, Y. J. Gu, Z. Y. Chen, and C. J. Li, J. Chem. Phys. **141**, 124201 (2015).
[27] J. Zheng, Q. F. Chen, Y. J. Gu, and Z. Y. Chen, Phys. Rev. E **86**, 066406 (2012).
[28] S. Root, R. J. Magyar, J. H. Carpenter, D. L. Hanson, and T. R. Mattsson, Phys. Rev. Lett. **105**, 085501 (2010).
[29] J. Zheng, Y. J. Gu, Z. Y. Chen, and Q. F. Chen, Phys. Rev. E **82**, 026401 (2010).
[30] W. J. Nellis, *Ultracondensed Matter by Dynamic Compression* (Cambridge University Press, Cambridge, UK, 2017).
[31] M. D. Knudson and M. P. Desjarlais, Phys. Rev. Lett. **118**, 035501 (2017).
[32] J. Weng, T. Tao, S. Liu, H. Ma, X. Wang, C. Liu, and H. Tan, Rev. Sci. Instrum. **84**, 113103 (2013).
[33] See Supplemental Material at http://link.aps.org/supplemental/10.1103/PhysRevB.97.140101, which includes Refs. [10,29,32,34–39,41–53], for (i) detailed descriptons of the experiment configuration and the diagnostic system, (ii) refractive index measurement of neon at the initial state, (iii) determination of the shock states, and (iv) detailed information of theoretical simulations.
[34] S. Root, K. R. Cochrane, J. H. Carpenter, and T. R. Mattsson, Phys. Rev. B **87**, 224102 (2013).
[35] M. D. Knudson, M. P. Desjarlais, R. W. Lemke, T. R. Mattsson, M. French, N. Nettelmann, and R. Redmer, Phys. Rev. Lett. **108**, 091102 (2012).
[36] G. E. Duvall and R. A. Graham, Rev. Mod. Phys. **49**, 523 (1977)
[37] Z. G. Li, Q. F. Chen, Y. J. Gu, J. Zheng, and X. R. Chen, AIP Adv. **6**, 105309 (2016).
[38] T. S. Duffy and T. J. Ahrens, J. Appl. Phys. **82**, 4259 (1997).
[39] N. C. Holmes, M. Ross, and W. J. Nellis, Phys. Rev. B **52**, 15835 (1995).
[40] M. D. Knudson, D. L. Hanson, J. E. Bailey, C. A. Hall, J. R. Asay, and C. Deeney, Phys. Rev. B **69**, 144209 (2004).
[41] V. Barone, M. Casarin, D. Forrer, M. Pavone, M. Sambi, and A. Vittadini, J. Comput. Chem. **30**, 934 (2009).
[42] S. Grimme, J. Chem. Phys. **124**, 034108 (2006).
[43] S. Grimme, J. Comput. Chem. **27**, 1787 (2006).
[44] W. L. Vos, J. A. Schouten, D. A. Young, and M. Ross, J. Chem. Phys. **94**, 3835 (1991).
[45] B. C. McGee, M. L. Hobbs, and M. R. Baer, Sandia Report No. SAND98-1191, 1998 (unpublished), https://www.osti.gov/servlets/purl/639774-2DQBBB/webviewable/.
[46] G. Kresse and J. Furthmuller, Phys. Rev. B **54**, 11169 (1996).
[47] G. Kresse and J. Hafner, Phys. Rev. B **49**, 14251 (1994).
[48] G. Kresse and J. Hafner, Phys. Rev. B **47**, 558 (1993).
[49] G. Kresse and J. Furthmuller, Comput. Mater. Sci. **6**, 15 (1996).
[50] P. E. Blochl, Phys. Rev. B **50**, 17953 (1994).
[51] G. Kresse and D. Joubert, Phys. Rev. B **59**, 1758 (1999).
[52] J. P. Perdew, K. Burke, and M. Ernzerhof, Phys. Rev. Lett. **77**, 3865 (1996).
[53] J. P. Perdew, K. Burke, and M. Ernzerhof, Phys. Rev. Lett. **78**, 1396 (1997).
[54] B. Militzer, Phys. Rev. B **79**, 155105 (2009).
[55] H. Sun, D. Kang, J. Dai, W. Ma, L. Zhou, and J. Zeng, J. Chem. Phys. **144**, 124503 (2016).
[56] G. W. Collins, P. M. Celliers, L. B. Da Silva, R. Cauble, D. M. Gold, M. E. Foord, N. C. Holmes, B. A. Hammel, R. J. Wallace, and A. Ng, Phys. Rev. Lett. **87**, 165504 (2001).